AIP Journal of Applied Physics

Defect engineered d 0 ferromagnetism in tin-doped indium oxide nanostructures and nanocrystalline thin-films

Gobinda Gopal Khan, Shyamsundar Ghosh, Ayan Sarkar, Guruprasad Mandal, Goutam Dev Mukherjee, Unnikrishnan Manju, Nasrin Banu, and Bhupendra Nath Dev

Citation: Journal of Applied Physics **118**, 074303 (2015); doi: 10.1063/1.4928952
View online: http://dx.doi.org/10.1063/1.4928952
View Table of Contents: http://scitation.aip.org/content/aip/journal/jap/118/7?ver=pdfcov
Published by the AIP Publishing

Defect engineered d^0 ferromagnetism in tin-doped indium oxide nanostructures and nanocrystalline thin-films

Gobinda Gopal Khan,[1,a),b)] Shyamsundar Ghosh,[2,a),b)] Ayan Sarkar,[1] Guruprasad Mandal,[3] Goutam Dev Mukherjee,[3] Unnikrishnan Manju,[4] Nasrin Banu,[5] and Bhupendra Nath Dev[5]
[1]*Centre for Research in Nanoscience and Nanotechnology, University of Calcutta, Technology Campus, Block JD-2, Sector III, Salt Lake City, Kolkata 700 098, India*
[2]*Department of Physics, Bejoy Narayan Mahavidyalaya, P.O. Itachuna, Hooghly 712 147, India*
[3]*Department of Physical Sciences, Indian Institute of Science Education and Research, Kolkata, Mohanpur Campus, BCKV Campus Main Office, Nadia 741 252, India*
[4]*Materials Characterization Division, CSIR-Central Glass and Ceramic Research Institute, 2A & 2B Raja S. C. Mullick Road, Jadavpur, Kolkata 700 032, India*
[5]*Department of Material Science, Indian Association for the Cultivation of Science, 2A & 2B Raja S. C. Mullick Road, Jadavpur, Kolkata 700 032, India*

(Received 3 December 2014; accepted 24 June 2015; published online 20 August 2015)

Origin of unexpected defect engineered room-temperature ferromagnetism observed in tin-doped indium oxide (ITO) nanostructures (Nanowires, Nano-combs) and nanocrystalline thin films fabricated by pulsed laser deposition has been investigated. It is found that the ITO nanostructures prepared under argon environment exhibit strongest ferromagnetic signature as compared to that nanocrystalline thin films grown at oxygen. The evidence of singly ionized oxygen vacancy (V_0^+) defects, obtained from various spectroscopic measurements, suggests that such V_0^+ defects are mainly responsible for the intrinsic ferromagnetic ordering. The exchange interaction of the defects provides extensive opportunity to tune the room-temperature d^0 ferromagnetism and optical properties of ITOs. © *2015 AIP Publishing LLC*. [http://dx.doi.org/10.1063/1.4928952]

I. INTRODUCTION

The d^0 ferromagnetism in oxide-based diluted magnetic semiconductors (DMS), induced by intrinsic crystalline defects and/or nonmagnetic impurities, opens up remarkable research opportunities for novel spintronics and magneto-optic device materials.[1,2] The discovery of room temperature ferromagnetism (RTFM) in pure HfO_2 thin films[3] demonstrates an interesting physics indicating that the oxide semiconductors can exhibit FM without the presence of any *d* or *f*-electrons, which is known as d^0 FM. Afterwards, numerous theoretical and experimental investigations have been conducted to study this new physical phenomenon for various pure and nonmagnetic element doped oxide semiconductor nanostructures and thin films.[4–9] Among various oxide semiconductors, tin-doped indium oxide (ITO) has drawn extensive research attention because of its versatile applications in nano-electronics, opto-electronics, sensor devices, and energy devices.[10–14] However, there are very few reports on the magnetic property of the pristine ITO thin films[15,16] and hardly any on its nanostructures. The study of magnetic properties of ITO is very exciting as it helps to manipulate both the spin and charge in a single material. Furthermore, there is also no clear correlation between the nature and origin of the observed FM for the ITO thin films. The origin of RTFM in the oxide semiconductors remains very controversial. For the transition metal (TM) doped DMSs, the great debate is whether the observed FM is appearing because of the intrinsic defects or from the segregation and the TM clusters in the semiconductor.[17] In case of the pure and nonmagnetic impurity doped oxides, various crystalline defects such as cation vacancies, oxygen vacancies, interstitial defects, and surface polarization have been demonstrated as the origin of FM.[6–9,15–20] Hence, along with the finding of new types of DMS, in depth understanding of the origin of the FM and the possible ways to tune the intrinsic magnetism of those materials are very significant considering their successful applications in spintronic devices.

Here, nanocrystalline thin films and various nanostructures (tiny nanowires (NWs), nano-comb, and NWs) of ITOs (90% In and 10% Sn) have been fabricated on the c-axis-sapphire ((0001) Al_2O_3) substrates by pulsed laser deposition (PLD) using different Ar and O_2 gas pressures (0.01, 0.1, and 1 mbar). All the ITOs exhibit RTFM, where FM of the ITO nanostructures is found to be higher than that of the nanocrystalline thin films. The origin of the RTFM in ITOs has been investigated by correlating the results of X-ray photoelectron spectroscopy (XPS), Photoluminescence (PL), Fourier transform infrared (FTIR) spectroscopy, and Raman spectroscopy with the observed FM signature from the magnetization measurements performed by superconducting quantum interference devices (SQUID). This study strongly suggests that the intrinsic RTFM of the ITO samples could be ascribed to the singly ionized oxygen vacancy (V_0^+, F^+ center) defects. The RTFM in ITOs also depends on the morphology of the samples because low dimension nanostructures having larger surface area are more prone to be enriched with considerable amount of surface defects (like

[a)]Authors to whom correspondence should be addressed. Electronic addresses: gobinda.gk@gmail.com, Tel.: +91 (033) 2335 0067 and sghoshphysics@gmail.com
[b)]G. G. Khan and S. Ghosh contributed equally to this work.

V_0^+ defects). However, there is ample opportunity to tailor the FM by tuning the intrinsic V_0^+ defects during the fabrication of materials.

II. EXPERIMENTAL SECTION

A. Synthesis of ITO samples

ITO nanostructures and nanocrystalline thin films are deposited by PLD technique on the c-axis-sapphire ((0001) Al_2O_3) substrate using a KrF excimer laser of laser power density $\sim 1.41\,J\,cm^{-2}$ and the pulse repetition rate of 5 Hz. The targets were prepared from high purity (99.998%) In_2O_3 and SnO_2 powders that are mixed with appropriate ratio (In:Sn = 9:1). The mixture is grinded well and then sintered at 800 °C. Pallets are prepared using a palletizer of 1 in. diameter. During deposition, the base pressure of the PLD chamber was maintained at 2×10^{-5} mbar, while the substrate temperature was fixed at 600 °C. Two sets of ITO samples are prepared. One set was prepared under pure oxygen (O_2) atmosphere at different oxygen pressures of 0.01, 0.1, and 1.0 mbar. While another set of ITO samples was prepared under the inert Ar gas atmosphere at pressure of 0.01, 0.1, and 1.0 mbar. The deposition time was 30 min for all the ITO samples. After the laser assisted deposition, the samples are annealed for 10 min under the same atmosphere and then cooled naturally at room temperature (RT).

B. Characterization of ITO samples

All the films are characterized by grazing incidence x-ray diffraction (GIXRD, X'Pert Pro, Panalytical) to reveal the crystallographic information of the samples. The morphology of the as prepared ITO samples is studied using a field emission scanning electron microscope (FESEM, FEI Quanta-200 Mark-2). The XPS (by using a PHI 5000 Versaprobe II Scanning XPS microprobe (ULVAC-PHI, USA)) has been employed to investigate the chemical compositions, valence state of the constituent elements and the intrinsic defects. The measurements were carried out at room temperature and at a base pressure better than 6×10^{-10} mbar. All the spectra were recorded with the monochromatic Al K_α ($h\nu = 1486.6$ eV) radiations with a total resolution of about 0.7 eV and a beam size of 100 μm. RT PL spectroscopic measurements were conducted to observe the band to band and defect-level transitions of the ITO samples by using a spectrofluorometer (Horiba Jobin Yvon, Fluorolog-3) having a Xe lamp source by using an excitation wavelength of 330 nm. The FTIR spectra were measured at RT in the range 400–800 cm^{-1} with a FTIR spectrometer (Jasco FTIR-6300) using the reflection methods. Raman spectroscopy measurements were carried out in the range of $50-1000\,cm^{-1}$ using a micro-Raman spectrometer (LABRAM HR from Horiba Jobin Yvon) at RT. Magnetic measurements are performed by SQUID magnetometer (7 T SQUID with an ever-cool dewar and vibrating sample magnetometer (Lakeshore, model 7144)).

III. RESULTS AND DISCUSSION

The effect of atmospheric condition on morphology and dimension of the as-prepared ITOs has been investigated by FESEM and is shown in Fig. 1. The ITO grown at 0.01 mbar of Ar pressure appears as the low aspect ratio vertically aligned NWs with squire-shaped tips (~80–100 nm, Fig. 1(a)). At Ar pressure of 0.1 and 1 mbar, the nano-comb (Fig. 1(b)) and high aspect ratio NWs (Fig. 1(c)) like ITO nanostructures are formed, respectively. A nano-comb consists of a solid stem (~70–80 nm) and perpendicular rod-like branches with ~40–50 nm diameters coming out of the stem. The diameter of the individual sharp tip long NWs (Fig. 1(c)) is found to vary from 70 to 30 nm along the length of the NWs. ITOs grown at different O_2 pressures appear as the nanocrystalline thin films containing the nano-pyramidal shape building blocks (Figs. 1(d)–1(f)). It is found that the dimension of the nano-pyramids increases with the increase of the O_2 pressure. The x-ray diffraction study of the ITOs, as shown in Fig. 2, indicates the good crystallinity of the samples with the presence of only In_2O_3 cubic bixbyite structure (JCPDS#17-2195), where no precipitation of SnO_2 is formed.

The PL spectra of the ITOs, shown in Figs. 3(a) and 3(b), are recorded to study the nature of defects present within the ITO lattice. All the ITOs are found to exhibit both UV and blue-green emissions. UV emission around 350 nm (~3.55 eV that is very close to In_2O_3 band gap energy) from the ITOs is believed to be because of the near band edge (NBE) radiative transitions related to the photogenerated electrons.[10,21] It is quite interesting to notice that the ITOs prepared in O_2 exhibit much stronger UV emission, while the ITOs deposited under Ar exhibit intense defect related PL emission at blue-green regime (390–500 nm). This contrasting behavior can be explained as the ITOs prepared in Ar are in the form of various one-dimensional (1D) nanostructures (as evident from FESEM); therefore, it is expected that they should have large surface area that contains more defects such as vacancies or surface defects, which can form various defect levels within the ITO band gap, and the electronic transitions between them can give rise to various defect-emissions at blue and blue-green zones. This leads to dominant mid-band emissions compared to the weak NBE UV emissions for the samples grown in Ar atmosphere. However, the ITOs prepared in O_2 (nanocrystalline thin films) having relatively large dimension (large surface area) should contain less amount of surface defects, and thereby UV emission dominates over the defect emission in these ITO thin-films. In addition, the oxygen-rich and oxygen-deficient atmosphere during the crystal growth can also impose a significant impact in modifying the defects within the samples. Due to the presence of an oxygen-deficient environment like Ar, the 1D ITO nanostructures should contain a large amount of oxygen vacancy defects and thereby can exhibit strong defect emission bands as observed here. In fact, the emission bands at blue and blue-green (390–500 nm) wavelength regions are due to various crystalline defects, such as surface defects and oxygen vacancies present in ITOs.[10,22,23] All the ITOs prepared in Ar exhibit two intense defect emissions around 420 and 436 nm, while these bands become quite insignificant for the ITO prepared in O_2. This observation certainly gives an indication that various oxygen vacancy defects (V_O^{++}, V_O^+, and V_O) are the

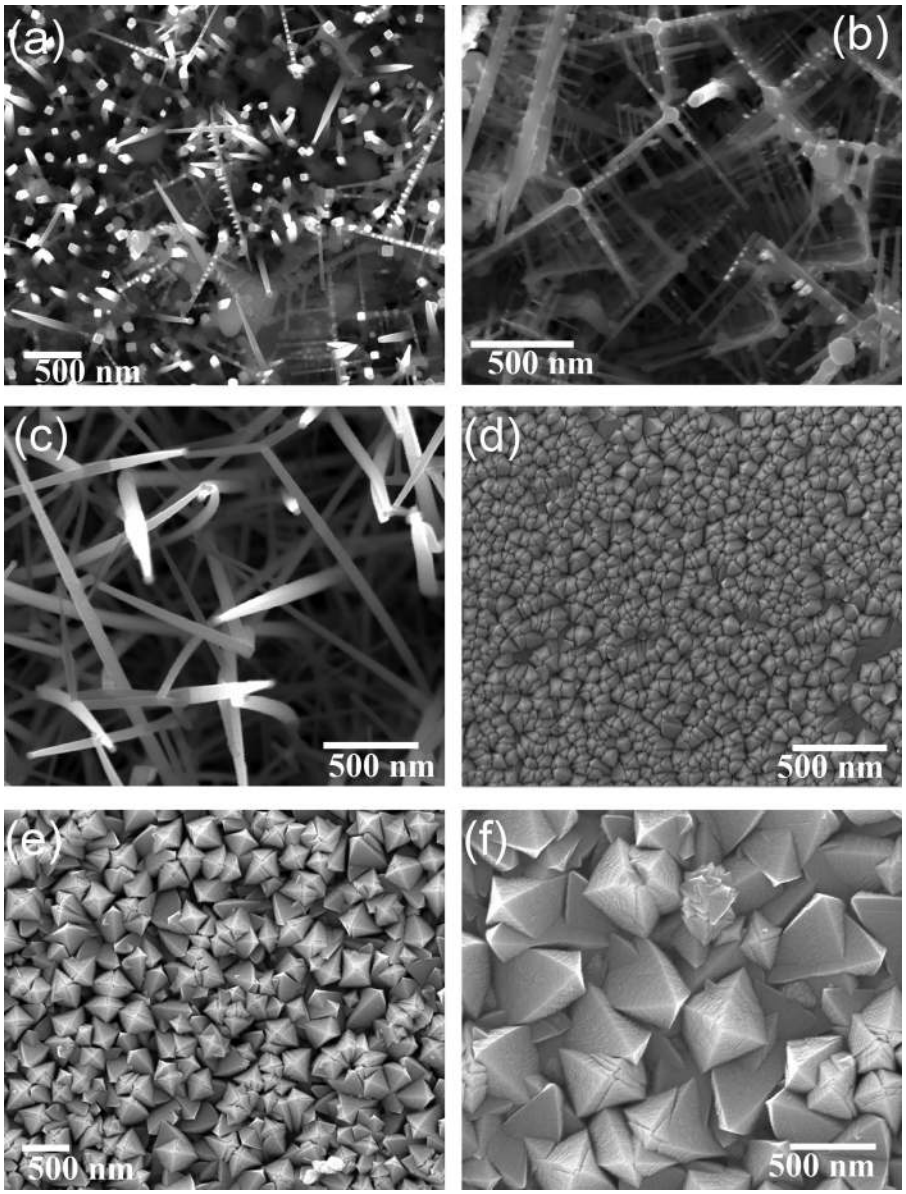

FIG. 1. FESEM images of ITO nanostructures and thin films deposited under Ar pressures of (a) 0.01, (b) 0.1, and (c) 1 mbar and O_2 pressures of (d) 0.01, (e) 0.1, and (f) 1 mbar.

origin of these two emissions. The defect emission from the ITOs near the blue (~420–425 nm) region is ascribed to the deep level singly ionized oxygen vacancy (V_0^+) defects,[10,23] whereas the band at (~436–440 nm) can be originated from other types of oxygen vacancy defects. The defect emission near 390 nm is correlated to the defect level introduced into the band gap of ITO because of the Sn doping as they introduce shallow trap states.[10] However, because of the loss of an O atom from ITO lattice, the electron pair that remains trapped in the oxygen vacancy cavity gives rise to an F center defect.[24] One of the electrons in F center is likely to occupy the neighboring In^{3+} ion (as the matrix is mostly rich with In) and generates a F^+ center (V_0^+), forming a mid band gap state in ITO. Thus, PL study reveals that the ITO nanostructures prepared under Ar atmosphere contain higher amount of oxygen vacancy defects compared with the nanocrystalline ITO thin films prepared at O_2 atmosphere.

Further investigation on the oxygen vacancy defects in ITOs has been conducted using XPS as it is a very effective tool to study surface defects in nanostructures. Figs. 4(a) and 4(b) show the XPS spectra of In 3*d* core level for ITOs prepared in Ar and O_2, respectively. The asymmetric nature and the broad shoulder towards the higher binding energy sides of the peaks indicate that each peak can be deconvoluted by two peaks (see Figs. 4(a) and 4(b)). Here, the peaks located at 445.5 and 453.1 eV having an energy difference of 7.6 eV correspond to In $3d_{5/2}$ and $3d_{3/2}$ orbitals, respectively, indicating the +3 oxidation state of In in ITOs.[25,26] The peaks located around the binding energies of 444.6 and 452.2 eV having an energy difference of 7.6 eV correspond to In $3d_{5/2}$ and $3d_{3/2}$ orbitals, respectively, which reveals the metallic nature of In,[25] suggesting that the indium should be present in lower oxidation state too. This result indicates that In^{3+} ions surrounded by oxygen vacancies might occupy electrons from the oxygen vacancy cavity and transform to the lower valency of In ion introducing a V_0^+ defects in ITO matrix. In Figs. 4(a) and 4(b), it is found that the ratio of intensity of In:In^{3+} for the ITO grown in Ar is higher than that grown in O_2, which clearly demonstrates that the samples grown in Ar have high concentration of V_0^+ defects compared with that

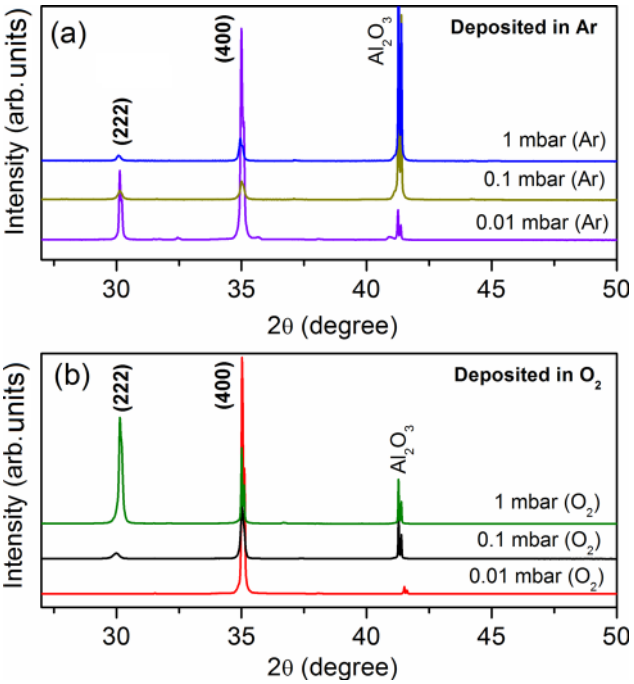

FIG. 2. The XRD patterns of the ITOs grown in (a) Ar and (b) O_2 using Cu K_α radiation.

grown in O_2. Furthermore, the intensity of In 3*d* core level spectra (Fig. 4(a)) for all the ITOs prepared in Ar looks alike, hence it is expected that there is little difference in the

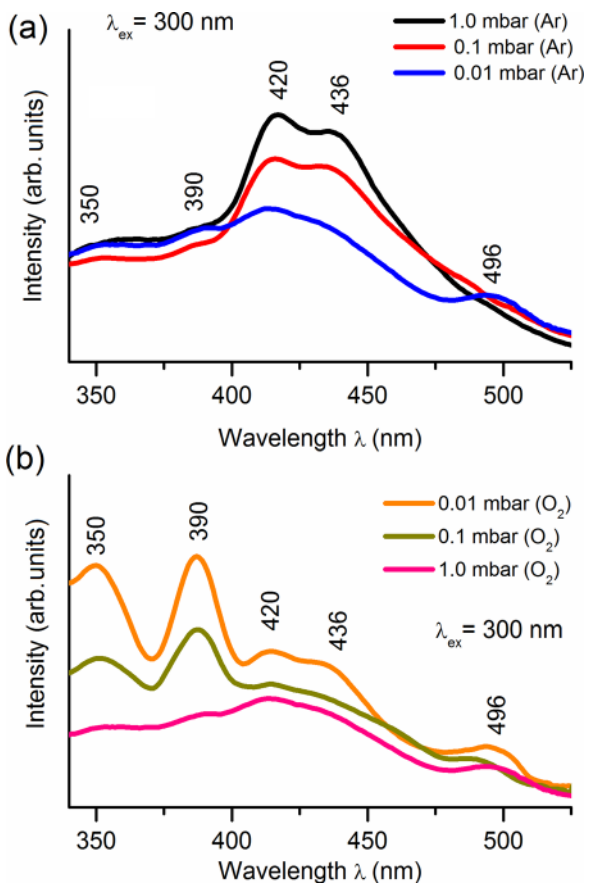

FIG. 3. Room temperature PL spectra of ITO nanostructures and TFs deposited in various (a) Ar and (b) O_2 pressures.

concentration of V_0^+ defects in them. It is found that the ratio of intensity of In:In^{3+} for the ITO grown in 1 mbar of O_2 is lower than that prepared in other O_2 pressures, which indicates that the ITO grown at 1 mbar of O_2 contains low concentration of V_0^+ defects compared with the samples prepared at low O_2 pressures. Figs. 4(c) and 4(d) show the XPS spectra of Sn 3*d* core level for ITOs prepared in Ar and O_2, respectively. The peaks look quite symmetrical centred at 486.4 and 494.9 eV corresponding to Sn $3d_{5/2}$ and $3d_{3/2}$ orbitals, respectively, indicating that the dopant Sn is in 4+ oxidation state.[25] The O 1*s* core level spectra (Figs. 4(e) and 4(f)) of the ITOs can also be deconvoluted by two peaks centred at 530.5 and 532 eV, corresponding to lattice oxygen in crystalline ITO and the oxygen deficient regions in lattice, respectively.[27,28] Interestingly, the intensity of the peak located at 532 eV is found to be less for the ITO prepared at 1 mbar of O_2 pressure compared with the samples prepared at low O_2 pressures, whereas there is little difference among the intensity of the 532 eV peaks for the ITOs prepared in Ar. This result also indicates that the high energy peak of the asymmetric O 1*s* core level spectra of ITOs is related to oxygen vacancy defects, which again reveals the presence of such defects in ITOs.

Raman spectroscopy is also employed in order to probe the oxygen vacancy defects growth of ITO nanostructures and thin films and is shown in Figs. 5(a) and 5(b). The cubic bixbyite structure of ITO is expected to exhibit 22 Raman active and 16 infrared active modes; however, only 6 Raman active modes have been observed in pure cubic single crystalline In_2O_3 and ITO nanostructures.[29] The Raman spectra of ITO nanostructures in the present study show 6 Raman modes at 103, 130, 306, 364, 499, and 612 cm^{-1}, which compares well with those observed in literature.[29] For cubic In_2O_3, the irreducible representation (IR) for the vibrational spectroscopy is given by $4A_g + 4E_g + 14T_g + 5A_u + 5E_u + 16T_u$.[29] The modes with symmetry A_g, E_g, and T_g are Raman active and infrared inactive. The vibrational modes T_u are infrared active and Raman inactive. The A_u and E_u vibrations are both Raman and infrared inactive.[29] The Raman mode at 130 cm^{-1} for ITOs is ascribed to the In-O vibrations of InO_6 octahedra.[29] The 306 and 499 cm^{-1} modes are demonstrated as the bending and stretching vibrations of InO_6 octahedra, respectively. In In_2O_3, 367 cm^{-1} peak is assigned to the stretching vibrations of the In-O-In in the unit cell of ITO. It is found that the vibration of In-O-In bond is greatly affected by the presence of V_0 defects. The change in intensity and shifting of Raman peak position is caused by such defects. Hence, the observed red shift of mode of In-O-In vibrations to 364 cm^{-1} for the ITOs can be attributed to the weaker binding forces due to creation of oxygen vacancies. Since the most dominant part in the Raman scattering intensity is proportional to the square of the derivative of the polarizability to the amplitude of the normal mode, creation of oxygen vacancies is expected to change the intensity of 364 cm^{-1} Raman mode. It can be seen in Fig. 5(a) that for the ITOs grown in Ar, the intensity of the 364 cm^{-1} peak with respect to the 130 cm^{-1} peak remains almost constant for all the samples, which indicates there is a little change in the concentration of V_0 defects in those ITO samples. Whereas, the similar change in the ITOs

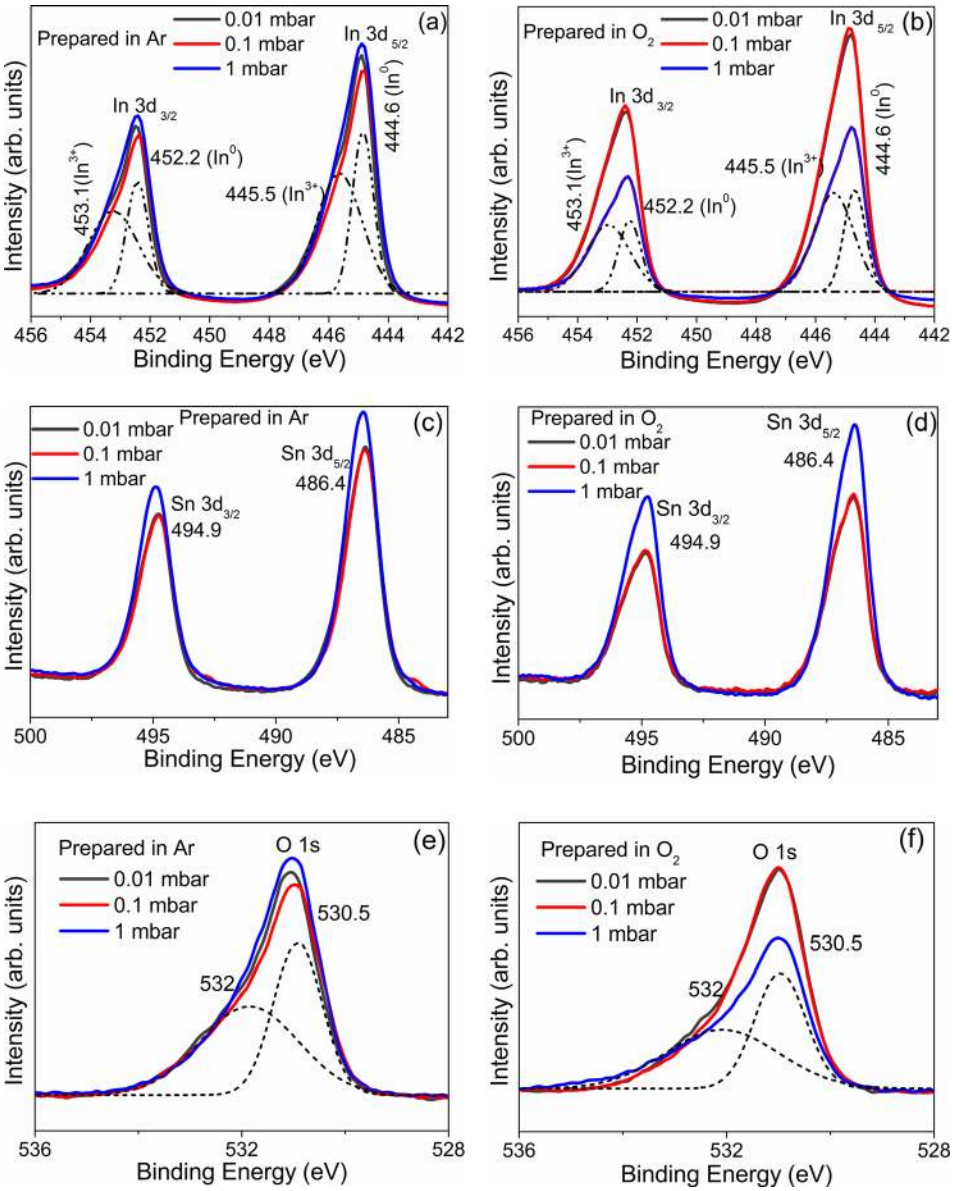

FIG. 4. XPS spectra of In 3*d* core level for the ITO samples prepared in various (a) Ar and (b) O_2 pressures. XPS spectra of Sn 3*d* core level for the ITOs prepared in various (c) Ar and (d) O_2 pressures. XPS spectra of O 1*s* core level for the ITOs prepared in various (e) Ar and (f) O_2 pressures.

grown in O_2 atmosphere is quite significant. For ITO prepared in 1 mbar of O_2, the relative intensity of the 364 cm^{-1} peak is very weak, indicating that the sample contains less amount of oxygen vacancies.[29]

Fig. 6 shows the FTIR reflectance spectra of the as-prepared ITOs at RT. In_2O_3 exhibits intense bands around 419 and 440 cm^{-1} attributed to In-O lattice stretching vibrations.[30,31] The ITO prepared at 1 mbar of O_2 pressure exhibits intense vibration peaks situated at 415 and 441 cm^{-1}, which correspond to 419 and 440 cm^{-1} vibration peaks, respectively, because of the In-O lattice vibrations of In_2O_3. For other ITO thin films, both the 415 and 441 cm^{-1} peaks are red shifted towards to lower wavenumber, and for the ITOs prepared in Ar, the peak positions become 412 and 437 cm^{-1}, respectively. The relatively more red shift of the In-O stretching vibration peaks in ITOs prepared in Ar compared with that prepared in O_2 is expected to the due to crystalline defects most likely higher concentration of oxygen vacancies induced during annealing in inert atmosphere.[9,32]

The RT field dependent magnetic (M–H) measurements of the ITOs are shown in Fig. 7(a). It is evident that the ITOs prepared both in Ar and O_2 exhibit significant ferromagnetic behavior with well-defined coercivity (H_C) and saturation magnetization (M_S). The temperature-dependent magnetization, M(T), curves for the ITOs prepared in different O_2 and Ar pressures are shown in Figs. 7(b) and 7(c), respectively. The variation of M_S and Curie temperature (T_C) of the ITOs prepared in different atmosphere pressures are shown in Figs. 7(d) and 7(e), respectively. Interestingly, the ITOs grown in Ar are found to exhibit larger magnetization and higher T_C compared to that deposited in O_2. Moreover, for the ITOs deposited in O_2-rich condition, the M_S is found to decrease significantly consistently with increasing of oxygen pressure. In this work, as no trace of magnetic impurities is detected, hence it is expected that the different inherent crystalline defects that stabilize during the crystal growth under various (Ar and O_2) experimental atmosphere must be responsible for such ferromagnetic behaviour in the low-dimensional ITO nanostructures. Similar type of RTFM has

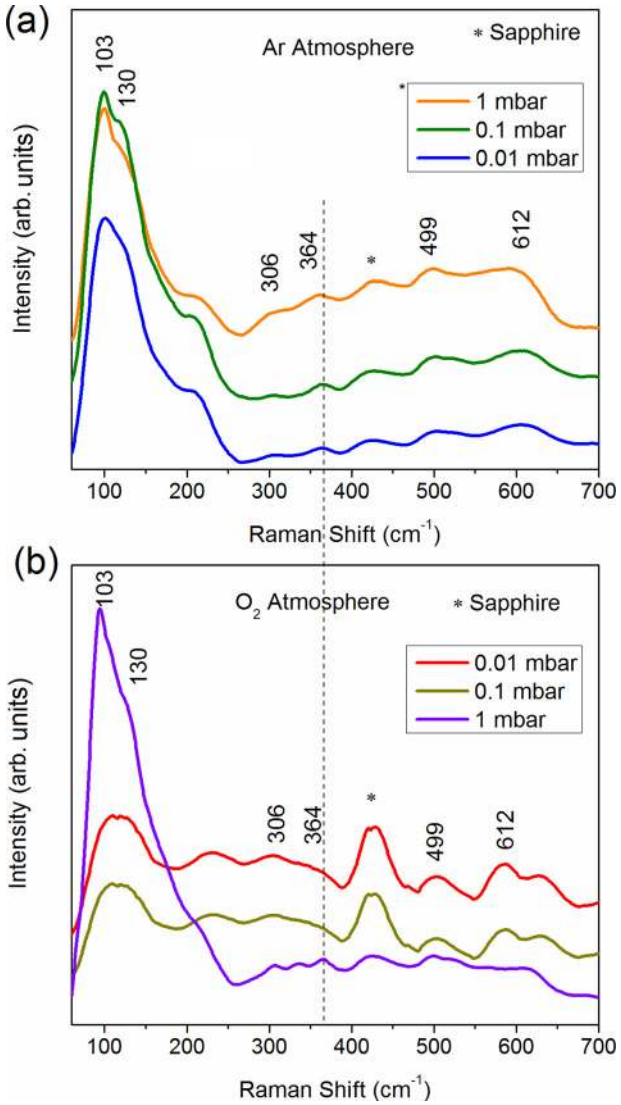

FIG. 5. Room temperature Raman spectra of ITO nanostructures and thin films prepared under (a) Ar and (b) O_2.

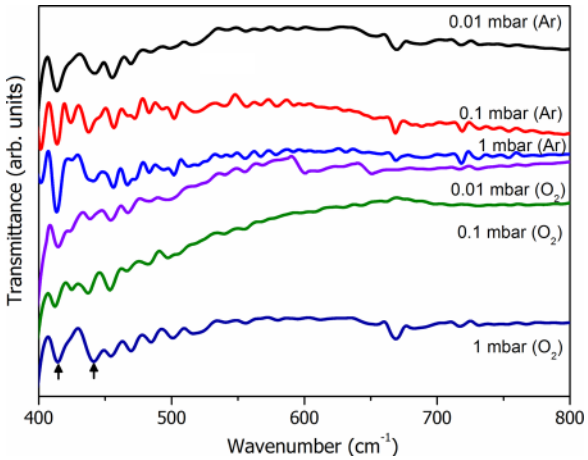

FIG. 6. FTIR spectra of ITO nanostructures and thin films prepared in Ar and O_2.

also been observed in other low dimensional wide band semiconductors, where the origin of FM was ascribed to several point defects.[6–9,15–20]

However, in order to understand the origin of RTFM in ITOs here, one should look back on earlier discussions related to PL, XPS, Raman, and FTIR spectroscopy studies. From the spectroscopic investigations, it is evident that the ITO nanostructures grown in Ar contain more amounts of oxygen vacancy defects than that of the ITO thin films grown in O_2. Interestingly, these ITO nanostructures grown in Ar also exhibit larger magnetic moment (M_S) compared to that grown in O_2. Hence, it is believed that oxygen vacancy defects are playing the key role in inducing ferromagnetism. Now, the question is how can such defects introduce ferromagnetism? Due to the loss of an O atom from ITO lattice, the electron pair that remains trapped in the oxygen vacancy cavity gives rise to an F center defect.[24] One of the electrons in F center is likely to occupy the neighboring In^{3+} ion and thus yields In^{2+} center and an F^{+} center (V_0^{+} defect) in the

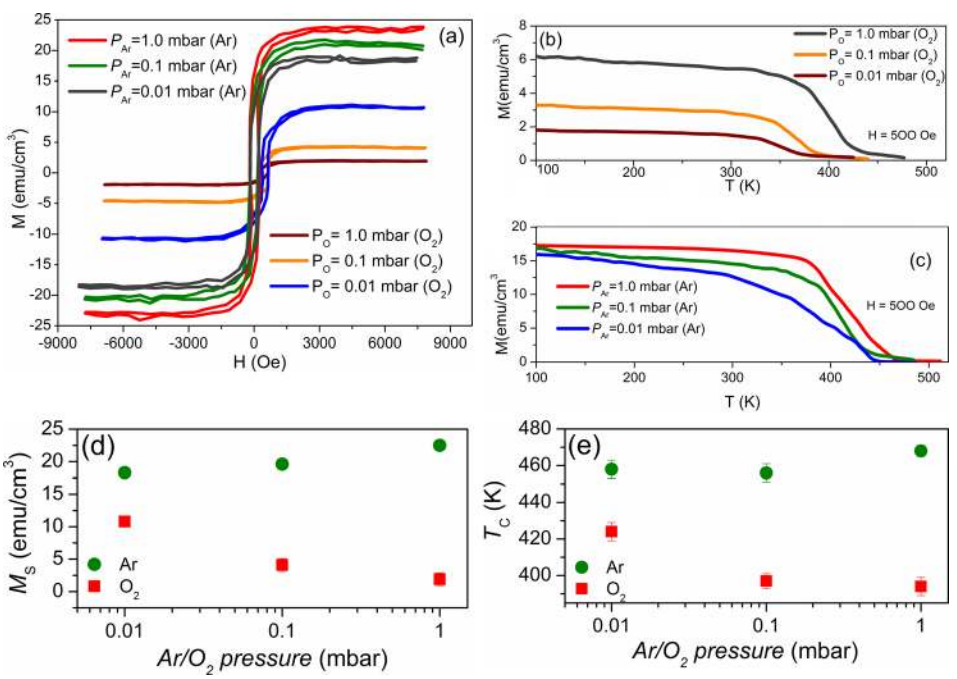

FIG. 7. (a) Room temperature M-H loops of different ITO samples deposited under Ar and O_2 atmosphere. Temperature-dependent magnetization curves for the ITO samples (b) and (c). Variation of saturation magnetization (*d*) and T_C (e) of ITOs with respect to O_2 and Ar pressures.

lattice.[24] The electron associated with such donor V_O^+ defect will be confined in a hydrogenic orbit[33] with radius, $r_H = \varepsilon(m/m^*)a_0$, where ε is the high-frequency dielectric constant, m is the electron mass, m^* is the effective mass of the donor electrons, and a_0 is the Bohr radius (53 pm). The magnetic moment ($\sim 1\mu_B$) of such trapped electron is localized at the center of the orbit.[33] As the concentration of oxygen vacancy defects increases in the specimen, more and more F^+ center orbit comes closer and finally overlaps to other when the concentration exceeds a percolation threshold favoring a long rage ferromagnetic interaction.[33,34] Besides V_O^+ defects, a cation vacancy such as indium vacancy (V_{In}) here, can also induce significant magnetic moment that generally arises from the *2p* orbital electrons of oxygen atom in the vicinity of V_{In}.[7,35,36] However, due to high formation energy, it is quite difficult to create and stabilize significant amount of V_{In} defects without any proper defect-engineering.[37] However, formation of V_O^+ defects is quite favorable especially when the ITOs are grown under an oxygen deficient condition like Ar.

Further correlation can be extracted if we look on the variation of M_S of the ITOs grown in O_2. The ITO nanopyramids grown at the lowest O_2 pressure (0.01 mbar) exhibit strongest magnetic moment because they contain higher amount of V_O^+ defects, as evident from the earlier spectroscopic details. It is also evident (from FESEM study) that the same film also contains the distribution of smallest nanocrystals among the ITOs grown in O_2. Hence, as the effective surface area of this film is much higher than that of others, it also contains high concentration V_O^+ defects at surface and grain boundaries. It is quite expected because the samples with lower dimension are prone to be enriched with more defects due to their higher surface area. However, ITO film grown in 1 mbar of O_2 pressure becomes quite a bulk type with small effective surface area and therefore low concentration of V_O^+ defects leading to weak FM. ITO nanostructures grown in Ar are found to exhibit almost similar magnitude of M_s because variation of Ar pressure cannot change the oxygen stoichiometry drastically, confirmed by XPS analysis. Still a trend of slow increase of M_S is observed when Ar pressure is changed from 0.01 to 1 mbar. This is again because of the dimensional change of the respective ITOs. It is found that with the increase of Ar pressure not only the morphology of ITO changes but also the dimension of the samples decreases consistently. Hence, the ITO NWs grown at highest Ar pressure (1 mbar) exhibit highest M_S because of its high surface area and consequently large concentration of surface V_O^+ defects. The studies reveal that the V_O^+ defects are responsible for stabilizing RTFM in ITOs, which can be tuned by changing deposition pressure and atmosphere. The strength of RTFM enhances as the concentration of V_O^+ defects increases in the ITO nanostructures and thin films.

IV. CONCLUSIONS

In summary, this work demonstrates the origin of RTFM of different ITO nanostructures and nanocrystalline thin films fabricated by PLD under various deposition pressure and atmosphere. Studies indicate that the different deposition gas pressures not only tailor the morphology and dimension of the ITOs but also control their inherent properties. Correlating the PL, XPS, FTIR, and Raman spectroscopy studies with magnetic measurements, it is found that the exchange interactions of singly ionized oxygen vacancies (V_O^+) are responsible for stabilizing RTFM in ITOs. The low dimensional ITOs nanostructures (nanocombs, nanowires) prepared under Ar are found to exhibit larger M_S and higher T_C due to the presence of large concentration V_O^+ defects within them. Among the ITO nanocrystalline thin films prepared under O_2, the strength of RTFM is found to diminish gradually with the increase of O_2 pressure due to decrease of V_O^+ defect concentration. Thus, this study shows that the RTFM in ITO nanostructures and nanocrystalline thin films can be tuned successfully by varying the PLD deposition pressure and atmosphere and that can put significant impact on the development of oxide-based spintronics and opto-spintronics.

ACKNOWLEDGMENTS

One of the authors, Gobinda Gopal Khan, is thankful to the Department of Science and Technology (DST), Government of India, for providing research support through "INSPIRE Faculty Award" (IFA12-ENG-09).

[1]G. A. Prinz, Science **282**(5394), 1660–1663 (1998).
[2]Y. Matsumoto, M. Murakami, T. Shono, T. Hasegawa, T. Fukumura, M. Kawasaki, P. Ahmet, T. Chikyow, S. Koshihara, and H. Koinuma, Science **291**(5505), 854–856 (2001).
[3]M. Venkatesan, C. B. Fitzgerald, and J. M. D. Coey, Nature **430**, 630 (2004).
[4]C. D. Pemmaraju and S. Sanvito, Phys. Rev. Lett. **94**, 217205 (2005).
[5]I. S. Elfimov, S. Yunoki, and G. A. Sawatzky, Phys. Rev. Lett. **89**, 216403 (2002).
[6]A. Sundaresan, R. Bhargavi, N. Rangarajan, U. Siddesh, and C. N. R. Rao, Phys. Rev. B **74**, 161306(R) (2006).
[7]S. Ghosh, G. G. Khan, S. Varma, and K. Mandal, J. Appl. Phys. **112**, 043910 (2012).
[8]G. G. Khan, S. Ghosh, and K. Mandal, J. Solid State Chem. **186**, 278–282 (2012).
[9]B. Santara, P. K. Giri, K. Imakitab, and M. Fujiib, Nanoscale **5**, 5476–5488 (2013).
[10]J. Gao, R. Chen, D. H. Li, L. Jiang, J. C. Ye, X. CMa, X. D. Chen, Q. H. Xiong, H. D. Sun, and T. Wu, Nanotechnology **22**, 195706 (2011).
[11]I. Hamberg and C. G. Granqvist, J. Appl. Phys. **60**, R123 (1986).
[12]M. Fang, A. Aristov, K. V. Rao, A. V. Kabashin, and L. Belova, RSC Adv. **3**, 19501 (2013).
[13]S. Ngamsinlapasathian, T. Sreethawong, Y. Suzuki, and S. Yoshikawa, Sol. Energy Mater. Sol. Cells **90**, 2129 (2006).
[14]Q. Wan, E. Dattoli, W. Fung, W. Guo, Y. Chen, X. Pan, and W. Lu, Nano Lett. **6**, 2909 (2006).
[15]B. Xia, Y. Wu, H. W. Ho, C. Ke, W. D. Song, C. H. A. Huan, J. L. Kuo, W. G. Zhu, and L. Wang, Physica B **406**(17), 3166–3169 (2011).
[16]H. S. Majumdar, S. Majumdar, D. Tobjörka, and R. Österbackaa, Synth. Met. **160**(3–4), 303–306 (2010).
[17]S. Ghosh, D. De Munshi, and K. Mandal, J. Appl. Phys. **107**, 123919 (2010).
[18]A. Janotti and C. G. Van de Walle, Rep. Prog. Phys. **72**(12), 126501 (2009).
[19]R. Podila, W. Queen, A. Nath, J. T. Arantes, A. L. Schoenhalz, A. Fazzio, G. M. Dalpian, J. He, S. J. Hwu, M. J. Skove, and A. M. Rao, Nano Lett. **10**(4), 1383–1386 (2010).
[20]T. Taniguchi, K. Yamaguchi, A. Shigeta, Y. Matsuda, S. Hayami, T. Shimizu, T. Matsui, T. Yamazaki, A. Funatstu, Y. Makinose, N. Matsushita, M. Koinuma, and Y. Matsumoto, Adv. Funct. Mater. **23**, 3140 (2013).
[21]H. Cao, X. Qiu, Y. Liang, and Q. Zhu, Appl. Phys. Lett. **83**, 761 (2003).

[22]C. L. Hsin, J. H. He, and L. J. Chen, Appl. Phys. Lett. **88**, 063111 (2006).
[23]X. S. Peng, G. W. Meng, J. Zhang, X. F. Wang, Y. W. Wang, C. Z. Wang, and L. D. Zhang, J. Mater. Chem. **12**, 1602–1605 (2002).
[24]N. Serpone, J. Phys. Chem. B **110**(48), 24287–24293 (2006).
[25]J. Ba, D. F. Rohlfing, A. Feldhoff, T. Brezesinski, I. Djerdj, M. Wark, and M. Niederberger, Chem. Mater. **18**(12), 2848–2854 (2006).
[26]B. V. Crist, *Handbooks of Monochromatic XPS Spectra* (XPS International, 1997).
[27]D. Maestre, A. Cremades, J. Piqueras, and L. Gregoratti, J. Appl. Phys. **103**, 093531 (2008).
[28]S. Y. Li, C. Y. Lee, P. Lin, and T. Y. Tseng, Nanotechnology **16**, 451–457 (2005).
[29]J. Gan, X. Lu, J. Wu, S. Xie, T. Zhai, M. Yu, Z. Zhang, Y. Mao, S. C. I. Wang, Y. Shen, and Y. Tong, Sci. Rep. **3**, 1021 (2013).
[30]M. Pashchanka, R. C. Hoffmann, A. Gurlo, and J. J. Schneider, J. Mater. Chem. **20**, 8311–8319 (2010).
[31]E. C. C. Souza, J. F. Q. Rey, and E. N. S. Muccillo, Appl. Surf. Sci. **255**, 3779–3783 (2009).
[32]K. Das, S. N. Sharma, M. Kumar, and S. K. De, J. Phys. Chem. C **113**, 14783–14792 (2009).
[33]J. M. D. Coey, M. Venkatesan, and C. B. Fitzgerald, Nature Mater. **4**, 173 (2005).
[34]S. Ghosh, G. G. Khan, and K. Mandal, ACS Appl. Mater. Interfaces **4**(4), 2048–2056 (2012).
[35]S. Ghosh, G. G. Khan, B. Das, and K. Mandal, J. Appl. Phys. **109**, 123927 (2011).
[36]G. Bouzerar and T. Ziman, Phys. Rev. Lett. **96**, 207602 (2006).
[37]C. Kilic and A. Zunger, Phys. Rev. Lett. **88**, 095501 (2002).